Recent developments in Monte Carlo simulations

Jennifer M. Thompson

IPPP, South Road, University of Durham, UK

This talk outlines the current status of Monte Carlo simulations in particle physics. It demonstrates the implementation of automated NLO contributions to matrix elements. The matching methods MC@NLO and POWHEG are outlined and results using various NLO tools are presented. The first plots from POWHEG showing the matching of NNLO matrix elements to the parton shower are also presented.

1. Introduction

There is a current drive in the Monte Carlo community to include higher order perturbative corrections in computational simulations. The most recent developments in Monte Carlos has been to include NLO QCD corrections to the matrix element matched to the parton shower.

Motivations for this extension are the occurrence of large and non-flat K-factors (σ_{NLO}/σ_{LO}), indicating the need for a local K-factor. Also, NLO matrix element calculations exhibit a significant reduction in scale dependence. In a Monte Carlo, extending the matrix element calculation to NLO QCD allows a reasonable error estimate to be formed. Furthermore, the matching of the NLO prediction to the parton shower gives the distribution of the hardest emission to NLO accuracy [1].

Numerical fixed order NLO matrix elements are calculated by using a method such as Catani-Seymour subtraction [2]. Details on the subtraction method for numerical matrix element calculations can be found at Ref. [3]. Equation (1) relates the NLO cross section, σ_{NLO}, to the differential born (B), virtual (V) and real (R) cross sections. The subtraction term introduced here is denoted by $B \otimes \mathrm{d}S$ as it can be factorised into the underlying Born configuration and a splitting function.

$$\sigma_{NLO} = \int \mathrm{d}\Phi_B \left[B + \int \mathrm{d}\Phi_1 B \otimes \mathrm{d}S + V \right] + \int \mathrm{d}\Phi_R \left[R - B \otimes \mathrm{d}S \right] \qquad (1)$$

Equation (1) allows for the numerical calculation of NLO matrix elements. However, including a parton shower on top of this requires a matching method such as the POWHEG [4] and MC@NLO [5] method.

2. POWHEG

Here we will briefly look at the formalism (for a more involved treatment, see Ref. [4]) and see some example plots from using the POWHEG method. The POWHEG implementations considered are from POWHEG-BOX [6], HERWIG++ [7] and PYTHIA8 [8].

2.1. POWHEG formalism

In order to include a possible matrix element emission, the Sudakov form factor is modified in the POWHEG formalism by identifying the kernel with the ratio of the real matrix element and the underlying born term.

$$\Delta(\mu, \mu_0) = \exp\left[-\int_{\mu_0}^{\mu} \mathrm{d}\Phi_1 \frac{R(\Phi_B \otimes \Phi_1)}{B(\Phi_B)}\right] \tag{2}$$

Equation (2) is then included in the POWHEG master equation (equation (3)) to reweight the contribution from the matrix element.

$$\sigma_{\mathrm{POWHEG}} = \int \mathrm{d}\Phi_B \overline{B}(\Phi_B) \left[\Delta(\mu, \mu_0) + \int_{\mu_0}^{\mu} \mathrm{d}\Phi_1 \frac{R(\Phi_B \otimes \Phi_1)}{B(\Phi_B)} \Delta(k_T^2, \mu_0)\right] \tag{3}$$

This gives a modified Born term, $\overline{B}$, which is the calculation to NLO, and correctly accounts for a possible matrix element emission. The phase space can be divided into 2 regions by introducing a small parameter. It is divided such that should this introduced parameter be taken to 0, the equation above is recovered. The advantage of this is that the new parameter can be tuned to match NNLO distributions or data [9].

2.2. Results from POWHEG

Figure 1 compares CDF data to Monte Carlo simulation for diphoton production. The Monte Carlo used here is HERWIG++ with the POWHEG method implemented. This shows the difference between the LO calculation and the NLO QCD matched sample. There is a substantially improved modelling of data, especially in the $\Delta\Phi$ plot.

Figure 2 shows the importance of NLO calculations in searches for BSM physics, as the affect on the distribution is clearly shown in the difference in magnitude of the dijet invariant mass peak on graviton events.

Higgs processes often contain local K-factors. Figure 2 shows the locality of the K-factor in the p_T of the 3^{rd} hardest jet in H+jets events. The effect of including NLO corrections on the scale uncertainties can also be seen here.

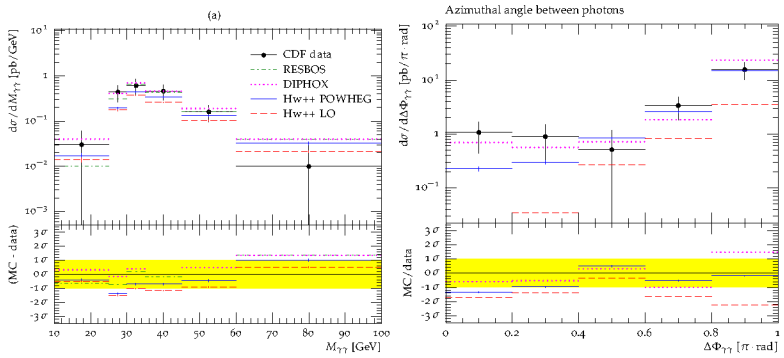

Fig. 1. The left hand plot shows the invariant mass of the photon pair with HERWIG+POWHEG compared to TeVatron data, and the right shows the $\Delta\Phi$ distribution of the pair. These plots are taken from Ref. [10].

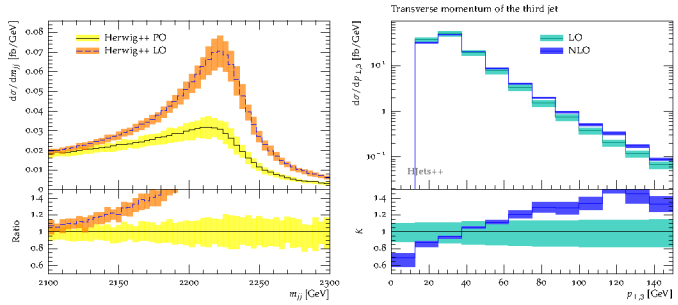

Fig. 2. The left hand plot shows the invariant mass of dijets in graviton production from Ref. [11], and the right hand plot shows the locality of the K-factor in the p_T distribution of the 3$^{\text{rd}}$ jet in Higgs production from Ref. [12].

3. MC@NLO

The MC@NLO method to match NLO matrix elements to a parton shower can be considered as a special case of a more general POWHEG method. For a detailed treatment, see Ref. [5]. In this section, some recent results using MC@NLO matching as implemented in aMC@NLO [13] and SHERPA [14] are presented.

3.1. MC@NLO formalism

This method extends the POWHEG master formula by splitting the real matrix element into a soft and a hard piece. The soft piece now contains the divergences of the matrix element, and the hard part represents the resolvable emission. The real contribution is formed from the sum of these

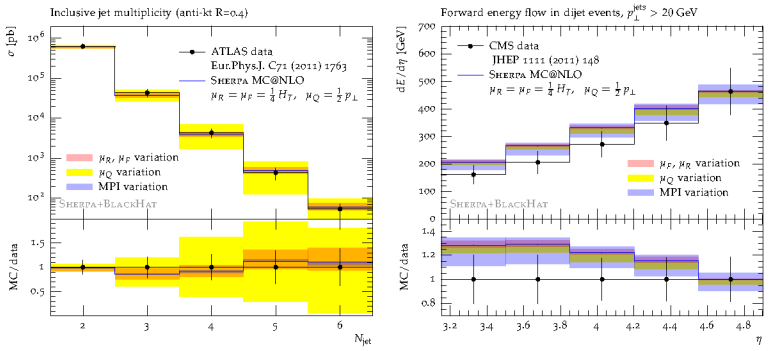

Fig. 3. This shows the a comparison of jet multiplicity in dijet events between SHERPA simulation and ATLAS (left) and of the forward energy flow in dijet events between SHERPA simulation and CMS (right). These plots are taken from Ref. [15]. The errors here are due to scale variation.

two pieces, $R = R^H + R^S$. R^H represents the hard piece and R^S represents the soft, divergent piece. This is then put back into the POWHEG master formula. This yields the MC@NLO master formula, Eq. (4).

$$\sigma_{\text{MC@NLO}} = \int \mathrm{d}\Phi_B \overline{B}(\Phi_B) \left[\Delta(\mu, \mu_0) + \int_{\mu_0}^{\mu} \mathrm{d}\Phi_1 \frac{R^S(\Phi_B \otimes \Phi_1)}{B(\Phi_B)} \Delta(k_T^2, \mu_0)\right] + \int \mathrm{d}\Phi_R R^H(\Phi_R) \quad (4)$$

The MC@NLO Sudakov form factor is

$$\Delta(\mu, \mu_0) = \exp\left[-\int_{\mu_0}^{\mu} \mathrm{d}\Phi_1 \frac{R^S(\Phi_B \otimes \Phi_1)}{B(\Phi_B)}\right] . \quad (5)$$

Equation (4) includes one additional term, which is the hard part of the real emission term. The modified matrix element is also altered by this separation. This introduces the possibility of negatively weighted events, which can introduce a small inefficiency. However, the splitting kernel in the Sudakov form factor can be used as the splitting kernel in the parton shower, making the transition from matrix element to parton shower natural. The MC@NLO method provides the hardest emission to NLO and introduces a local K-factor, similar to POWHEG.

3.2. MC@NLO Results

Figure 3 show ATLAS and CMS results for dijet events. The ATLAS jet multiplicity plot shows SHERPA+BLACKHAT [16] in good agreement with

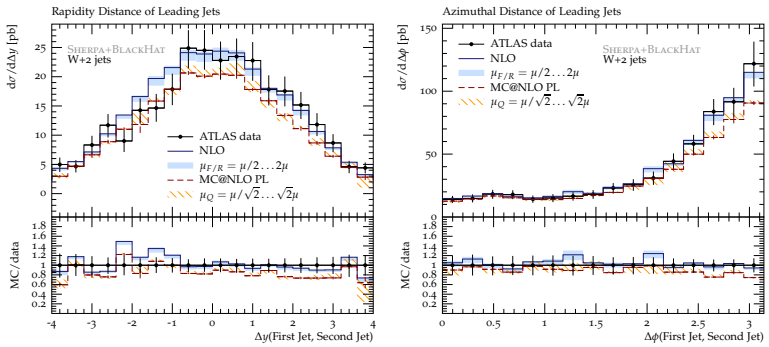

Fig. 4. These plots are from Ref. [17]. The distributions are of the hardest 2 jets in W boson production. The left hand plot is of Δy_{jj} and the right is of $\Delta\Phi_{jj}$.

the data, and the dominating uncertainty here comes from the variation in the resummation scale. The forward energy flow shows a prediction from SHERPA which is consistent with the data. Here the dominating error comes from the MPI.

Figure 4 uses SHERPA+BLACKHAT with W+2 jets production calculated with the MC@NLO method. This compares ATLAS data with NLO and MC@NLO simulations. The uncertainty on the fixed order prediction is given by a variation of renormalisation (μ_R) and fatorisation scale (μ_F) as $\frac{1}{2}\mu_{R/F} < \mu_{R/F} < 2\mu_{R/F}$. On the MC@NLO sample, the uncertainty is given by a variation of resummation scale, $\frac{1}{\sqrt{2}}\mu_Q < \mu_Q < \sqrt{2}\mu_Q$.

4. Merging methods

The matching methods considered above give the hardest emission correct to NLO. This can be considered alongside the merging methods, which better describe hard emissions than the parton shower, which becomes exact in the soft-collinear approximation. Merging methods are implemented in Monte Carlos at LO, and can be easily extended to NLO in principle, by a reweighting of all the contributing terms by a K-factor.

The merging methods considered here are MEPS@NLO [18], which is the implementation in SHERPA with MC@NLO, and MINLO [19], which is implemented with POWHEG.

4.1. Merging Results

This section presents results from merging NLO matrix elements together. Some of the plots show the improved modelling of the hard jets

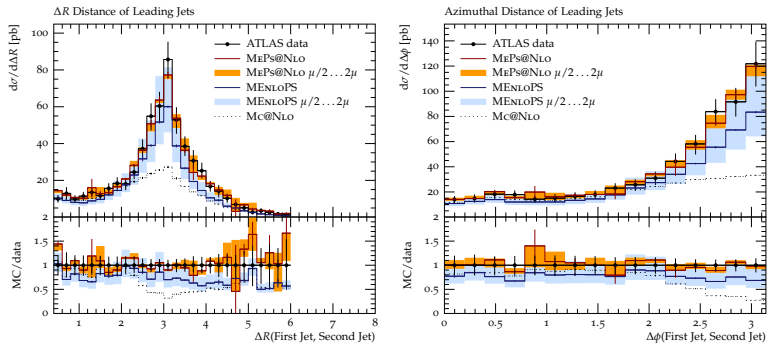

Fig. 5. These are SHERPA+BLACKHAT plots for the ΔR (left) and $\Delta\Phi$ (right) distributions between the hardest 2 jets in merged W+jets results from Ref. [20].

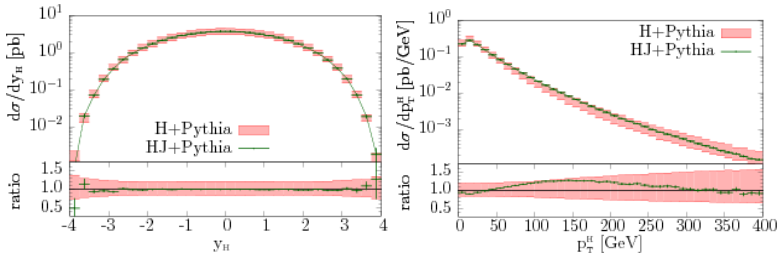

Fig. 6. The left hand plot shows the MINLO merged prediction for the Higgs rapidity, and the right hand plot shows the MINLO merged prediction for the p_T of the Higgs boson from Ref. [21].

that this achieves over simply a matching method. These improvements are most noticeable in observables sensitive to jets other than the hardest.

Figure 5, compares the different NLO techniques for ΔR and $\Delta\Phi$ distributions between the hardest 2 jets. The improvement as we move towards MEPS@NLO is very pronounced for these observables. This is due to how sensitive they are to the modelling of the second jet. MEPS@NLO is the only method which calculates this to NLO accuracy.

Figure 6 demonstrates the implementation of the MINLO method in PYTHIA with the POWHEG method. Figure 6 shows the difference between merging and POWHEG for the rapidity distribution of the Higgs boson in H+jets events. Here the first jet is merged in via the MINLO procedure. Figure 6 also shows the p_T distribution for the Higgs boson, again in H+jets events. Again, the comparison is made between POWHEG and the merging in of an additional jet.

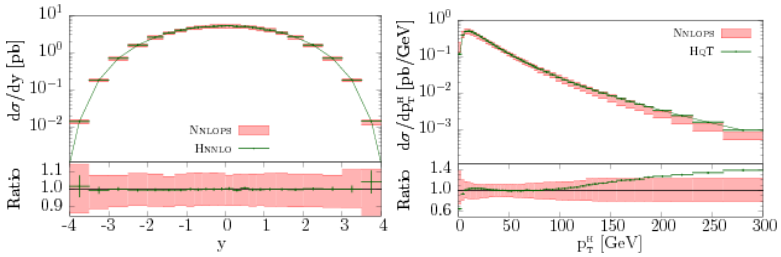

Fig. 7. The p_T and y of the Higgs boson is shown to NNLO matched to a parton shower. These plots are taken from Ref. [22].

5. NNLO matched to parton shower

POWHEG has recently released plots from the first instance of NNLO matrix elements being matched to parton shower [22]. These results are shown in Fig. 7, and are again for the rapidity and p_T of the Higgs boson in Higgs production processes. These can be compared with the POWHEG results for the same observables in Fig. 6. The uncertainties in Fig. 7 are greatly reduced, as compared with Fig. 6.

6. Future outlook and conclusions

In the near future, the NLO calculations performed in the Monte Carlo community will be compared with data once these become available, in order to fully verify our implementations of the NLO physics. Completing this leads naturally on to calculating higher order corrections on the longer term. This involves calculating NNLO QCD corrections, and also to begin to introduce NLO EW corrections which can become very large at the collider energies we are beginning to probe.

Another area of interest to the Monte Carlo physics community is to discuss observables which would help the community to properly understand what the Monte Carlo is doing in complicated regions of phase space, and for us to gain a deeper understanding of the physics involved in the processes we are modelling. To this end, the Monte Carlo community is discussing different measurements that we would like the experimentalists to complete.

The current status of Monte Carlo physics is the automation of NLO corrections to the vast majority of processes. These predictions have been compared to data in several cases, and even more are still being verified. The interfacing technology between the matrix element and the parton shower is now very well established.

Acknowledgments

This work is supported by STFC and MCnet. I would like to thank Dr. F. Krauss for his supervision and the University of Durham for their support. Also, I am grateful to the POWHEG-BOX and HERWIG++ Collaborations for providing some recent results.

References

[1] S. Höche, F. Krauss, M. Schönherr, and F. Siegert, J. High Energy Phys. **04**, 024 (2011).

[2] S. Catani and M. Seymour, Nucl. Phys. B **485**, 291 (1997).

[3] R.K. Ellis, D.A. Ross, and A.E. Terrano, Nucl. Phys. B **178**, 421 (1981).

[4] P. Nason, J. High Energy Phys. **11**, 042 (2004).

[5] S. Frixione and B. Webber, J. High Energy Phys. **06**, 029 (2002).

[6] P. Nason, arXiv:1001.2747.

[7] M. Bahr, *et al.*, arXiv:0803.0883.

[8] T. Sjöstrand, S. Mrenna, and P. Skands, arXiv:0710.3820.

[9] S. Alioli, P. Nason, C. Oleari, and E. Re, J. High Energy Phys. **04**, 002 (2009).

[10] L. D'Errico and P. Richardson, J. High Energy Phys. **02**, 130 (2011).

[11] A. Wilcock and P. Richardson, Eur. Phys. J. C **74**, 2713 (2014).

[12] F. Campanario, T.M. Figy, S. Plätzer, and M. Sjödahl, Phys. Rev. Lett. **111**, 211802 (2013).

[13] http://amcatnlo.cern.ch

[14] T. Gleisberg, *et al.*, J. High Energy Phys. **02**, 007 (2009).

[15] S. Höche and M. Schönherr, Phys. Rev. D **86**, 094042 (2012).

[16] C. Berger, *et al.*, Phys. Rev. D **78**, 036003 (2008).

[17] S. Höche, F. Krauss, M. Schönherr, and F. Siegert, Phys. Rev. Lett. **110**, 052001 (2013).

[18] S. Höche, F. Krauss, M. Schönherr, and F. Siegert, J. High Energy Phys. **04**, 027 (2013).

[19] K. Hamilton, P. Nason, and G. Zanderighi, J. High Energy Phys. **10**, 155 (2012).

[20] A. Höche, F. Krauss, M. Schönherr, and F. Siegert, J. High Energy Phys. **04**, 027 (2013).

[21] K. Hamilton, P. Nason, C. Oleari, and G. Zanderighi, J. High Energy Phys. **05**, 082 (2013).

[22] K. Hamilton, P. Nason, E. Re, and G. Zanderighi, J. High Energy Phys. **10**, 222 (2013).